High-pressure structural study of Tantalum pentoxide Ta_2O_5

Elissaios Stavrou,[1] Joseph M. Zaug,[1] Sorin Bastea,[1] and Martin Kunz[2]

[1)] *Lawrence Livermore National Laboratory, Physical and Life Sciences Directorate, P.O. Box 808 L-350, Livermore, California 94550, USA*

[2)] *Advanced Light Source, Lawrence Berkeley Laboratory, Berkeley, California 94720, United States*

(Dated: 6 February 2017)

Tantalum pentoxide Ta_2O_5 with the orthorhombic L-Ta_2O_5 structure has been experimentally studied under high pressure using synchrotron angle-dispersive powder x-ray diffraction (XRD) in a diamond-anvil cell up to 28.3 GPa (at room temperature). The ambient pressure phase remains stable up to 25 GPa followed by a pressure-induced amorphization above this pressure. A detailed Equation of state (EOS), including lattice parameters evolution with pressure, is reported. The results of this study were compared with a previous high-pressure XRD study in the same compound by Li *et al.* A clear discrepancy between the ambient-pressure crystal structures and, consequently, the reported EOSs between the two studies was reveled. The origin of this discrepancy is discussed in the context of the different crystal structures used to index the XRD patterns.

I. INTRODUCTION

Tantalum pentoxide Ta_2O_5 has been extensively studied mainly due to its high refractive index, making it suitable for optical coating,[1] and its wide bandgap (Eg = 4 eV) and dielectric constants, making suitable in electronic applications such as capacitors.[2] Moreover, the properties of Ta_2O_5 are important for a number of practical applications, including some, e.g. energetic materials, that require knowledge of its high pressure equation of state (EOS). Classical energetic materials are organic molecular compounds such as TNT, PETN, HMX, etc., which have a wide range of industrial and military uses due to their stored and easily available chemical energy. An attractive way of increasing the energy density of these materials is through the addition of metallic powders, which can provide significantly more energy through oxidation. Aluminum (Al), silicon (Si), boron (B) have been widely studied in this context, and with the advent of nanopowder production technologies, many other metals are currently being considered.[3,4] In the nanometer domain even nominally refractory metals such as tantalum (Ta) may be amenable to explosives and propellants applications[4] Ta and its oxidation have already been studied for example in thermite reactions.[5] Understanding and modeling the behavior and effects of metal fuels under these usage scenarios requires information on the properties of their oxides, including in particular the EOS. Experimental measurements of the structure and equation of state of Ta_2O_5 at moderate pressures are however rather scarce, despite ongoing interest in its shock properties under low initial density conditions, e.g. powders and aerogels.[6,7]

The crystal structure of tantalum pentoxide at ambient conditions has been under long debate, mainly due to the difficulty to grow high quality single crystals. Nevertheless, two, so-called "low-temperature", ambient conditions crystal structures are widely accepted in the literature:[8,9] a) the orthorhombic *P2mm* (S.G. 25, Z=11, PDF-71-639) L-Ta_2O_5[10] and b) the orthorhombic *Pccm* (S.G. 49, Z=2, PDF-01-070-9177) β-Ta_2O_5.[11] Moreover, a plethora of high-temperature structures have been reported. Here, for the shake of simplicity, we will only refer to the orthorhombic *Pmm2* (S.G. 25, Z=12, PDF-79-1375) T-Ta_2O_5 structure synthesized by Hummel *et al.*[12] through high temperature chemical procedures using an intermediate TT-Ta_2O_5 phase as percussor. L-Ta_2O_5 and T-Ta_2O_5 share common structural characteristics which are the presence of edge and corner sharing TaO_6 octahedra and TaO_7 pentagonal bipyramids.[10,12,13] Ta and O atoms form O-Ta-O layers in the *ab* plane and

along the c axis. The TaO_6 octahedra and TaO_7 pentagonal bipyramids of adjacent layers are connected by corner sharing along the c axis, see Fig. 1. In contrast, only corner sharing TaO_6 octahedra are present in the β-Ta_2O_5 structure,[11] see Fig. 1(b).

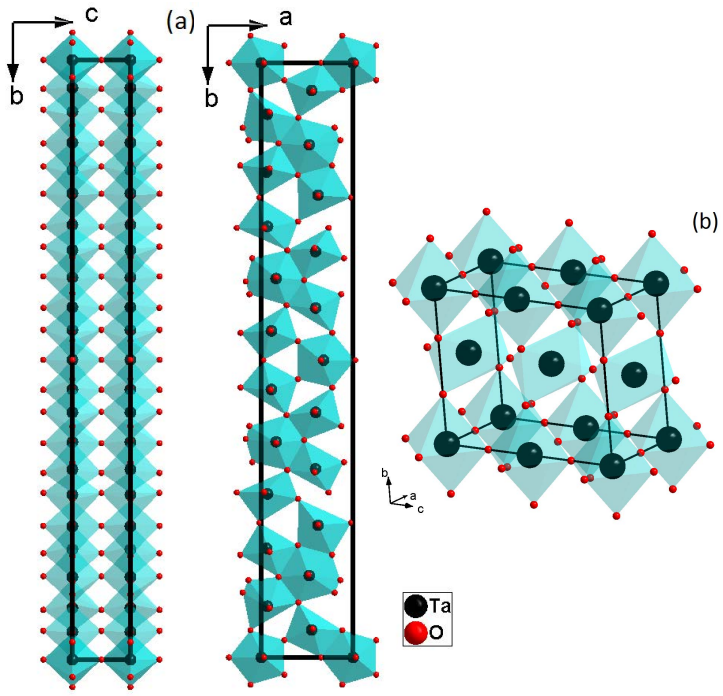

FIG. 1. Schematic representations of: a) the L-Ta_2O_5 structure along the a (left) and c (right) axis and b) the β-Ta_2O_5.

To our knowledge, only one high pressure study on bulk Ta_2O_5 has been published, by Li *et al.*[13] using in situ synchrotron X-ray diffraction (XRD) and Raman spectroscopy. In the same study the EOS of Ta_2O_5 up to 12 GPa, including lattice parameters evolution with pressure, was reported. Moreover, a pressure induced structural transition of the starting orthorhombic phase to an amorphous form in the pressure range of 18.4 - 24.7 GPa has been observed. In this study, although the authors state that they present a high pressure study of the low-temperature orthorhombic Ta_2O_5 the reported cell volume and lattice parameters are in strong disagreement with the ones reported by either Stephenson *et al.*[10] or by Aleshina *et al.*.[11] In contrast the T-Ta_2O_5 structure has been adopted to index the XRD patterns. We believe that this in an important shortcoming that should be corrected, not only for the accurate knowledge of the EOS of Ta_2O_5, but also because future studies in other systems maybe based on the results reported by Li et al. In order to resolve this issue, we have carried

out a detailed synchrotron angle-dispersive powder XRD study of Ta_2O_5 up to 28.3 GPa. We show that the XRD patterns of commercially available Ta_2O_5 can be well indexed with the low temperature orthorhombic L-Ta_2O_5 in agrement with Stephenson *et al.*.[10] Moreover, we report a detailed EOS of the L-Ta_2O_5 up to 25 GPa and a pressure induced amortization above this pressure.

II. METHODS

High purity commercially available (>99.99% CERAC, INC.) Ta_2O_5 was ground to fine powder for x-ray diffraction (XRD) measurements. The sample including pressure sensors were loaded into diamond-anvil cell (DAC) sample chambers. Rhenium gaskets (preindented to 40-45 μm thick using 400 μm diameter culets) were used to radially confine the pressurized samples. Initial sample chambers diameters were nominally 150 μm. Ne was utilized as a pressure-transmitting medium (PTM) for XRD. Pressure was determined using a known ambient temperature EOS of gold[14] and also using a calibrated ruby luminescence scale.[15] Image plate CCD detector was used to collect pressure dependent X-ray diffraction data at the Advanced Light Source Beamline 12.2.2. An X-ray wavelength of $\lambda = 0.4959$Å was selected using a Si(111) double-crystal monochromator. Exposures time varied between 10 and 30 secs. The sample to detector distance of 300 mm was determined using a CeO_2 (or LaB_6) diffraction pattern. The X-ray beam was focused to 10 x 10 μm using Kirkpatrick-Baez mirrors. More details on the experimental set up are given in Kunz *et al.*.[16]

Integration of powder diffraction images to yield scattering intensity versus 2θ patterns and initial analysis were performed using the DIOPTAS[17] program. Calculated XRD patterns were produced using the POWDER CELL program,[18] for the corresponding crystal structures according to the EOSs determined experimentally in this study and the published crystalline structures and assuming continuous Debye rings of uniform intensity. Le Bail refinements were performed using the GSAS[19] software. Indexing of XRD patterns has been performed using the DICVOL program[20] as implemented in the FullProf Suite.

III. RESULTS AND DISCUSSION

Fig. 2(a) shows the comparison between the experimental XRD pattern of Ta_2O_5 with the calculated pattern of L-Ta_2O_5 at ambient pressure. An almost perfect match, apart from a slight difference in relative intensities, is clearly observed. This is better highlighted in the Rietveld refinement of Fig. 2(b). The cell volume and the lattice parameters obtained for Ta_2O_5 in this study are in excellent agrement with the ones reported by Stephenson *et al.* for L-Ta_2O_5, see Table I. Figure 3 shows integrated diffraction patterns of Ta_2O_5 at selected pressures up to 28.3 GPa. Upon pressure increase L-Ta_2O_5 remains stable up to 26.5 GPa followed by a pressure induced amorphization at higher pressures, see Fig. 3. With full pressure release the amorphization is only partially lifted.

From the XRD data of Ta_2O_5, we have obtained the lattice parameters and the cell volume as functions of pressure, see Fig. 4. We were not able to determine the positional parameters for all atoms (*i.e.* only the positional parameters of Ta cations were refined during the Rietveld refinement), and consequently the interatomic distances, due to: a) the large difference in the Z values between Ta and O and b) the huge number (>100) of free positional parameters. The results are compared with the ones published by Stephenson *et al.* shown in Figures 4. Close inspection on the compressibility of the normalized lattice parameters (Fig. 4(a)) reveals a much higher compressibility along the c-axis, reflecting the higher compressibility perpendicular to the layers, see Fig. 1(a)). Moreover, a slight decrease of the compressibility of all axes is observed above ∼22GPa. Consistent with most high-pressure EOS studies, we conducted unweighted fits of the pressure-volume data, up

TABLE I. Experimental structural parameters of L-Ta_2O_5 and T-Ta_2O_5 phases of Ta_2O_5 at ambient pressure. Listed parameters include space group (SG), number of formula units in the unit cell Z, lattice parameters and cell volume.

Reference	Crystal structure	SG	Z	a(Å)	b(Å)	c(Å)	V(Å^3)
Stephenson et al.	L-Ta_2O_5	*P2mm*	11	6.198	40.29	3.888	970.201
Hummel *et al.*	T-Ta_2O_5	*Pmm2*	12	43.996	3.894	6.209	1063.75
Li *et al.*	T-Ta_2O_5	*Pmm2*	12	43.997	3.894	6.209	1063.75
This study	L-Ta_2O_5	*P2mm*	11	6.197	40.32	3.813	972.87

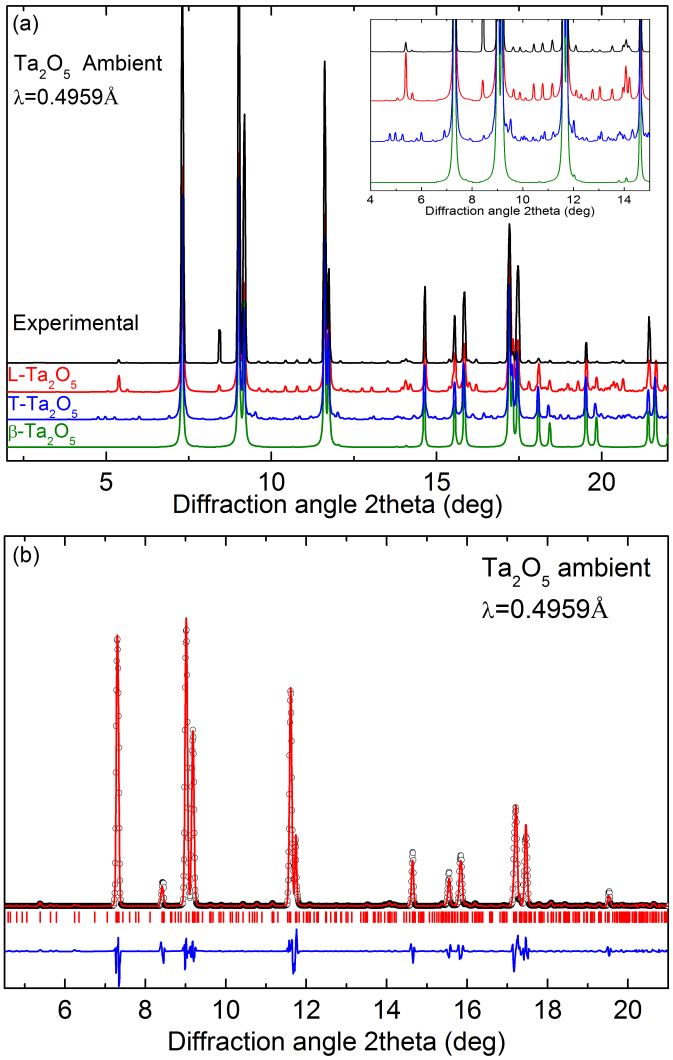

FIG. 2. (a)Calculated XRD patterns of L-Ta_2O_5, β-Ta_2O_5 and T-Ta_2O_5 at ambient pressure. The experimental XRD pattern of this study is also shown. (b) Rietveld refinement results for Ta_2O_5 at ambient pressure, L-Ta_2O_5 structure. Symbols correspond to the measured profile, the red solid lines represent the results of Rietveld refinements. The difference curve (blue curve) is shown also. Vertical tick marks indicate Bragg peak positions.

to 22 GPa, to a third- and second-order Birch-Murnaghan (B-M) equations of state[21] and determined the bulk modulus K_o and its first derivative K' (for the third-order B-M) at zero pressure for the L-Ta_2O_5. The elastic parameters obtained this way are: a) K_o= 199±2GPa and K'=0.1 for the third-order B-M and b) K_o= 160±5GPa for the second-order B-M. We postpone the discussion about the very low value of the K' as determined by the third-order B-M however, we would like to note that the results of the third-order B-M fit should be

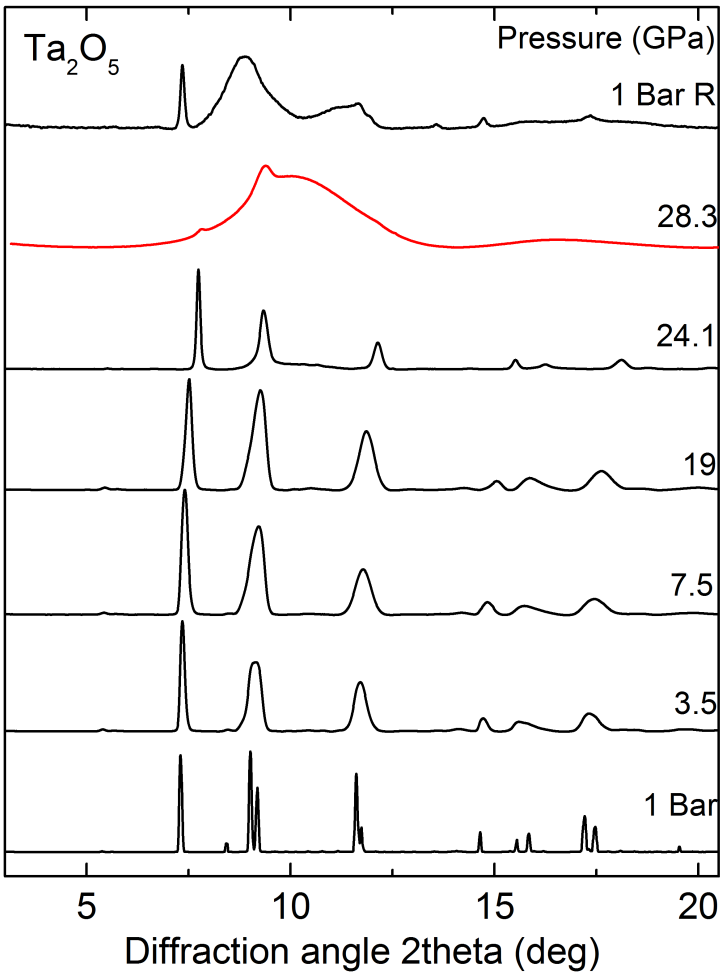

FIG. 3. XRD patterns of Ta_2O_5 at selected pressures.

only considered as indicative of a low K', given that its applicability range is limited to K' $\geq$4.

To gain deeper insight into how Ta_2O_5 responds under quasi-static compression, we conducted weighted fits and used the reduced χ^2_{red} goodness-of-fit formalism to compare the effectiveness of three EOS models to represent the P-V data. The reduced χ^2 value closest to 1 represents the best-fit model, see Ref.[22] for a complete description of the procedure. The Birch-Murnaghan,[21] (B-M), 2^{nd} to 4^{th} orders, the Vinet,[23] and the F-f[24] finite strain 1^{st} order EOS models were fit to the data, see fig. 5. Corresponding two-dimensional confidence ellipses are plotted for the best fit model to reveal two-variable correlation information (See Figs. 6(a) and 6(b)). Bivariable confidence plots enable a more comprehensive basis for comparison of EOS parameters to alternative theoretical and/or experimental results.[25]

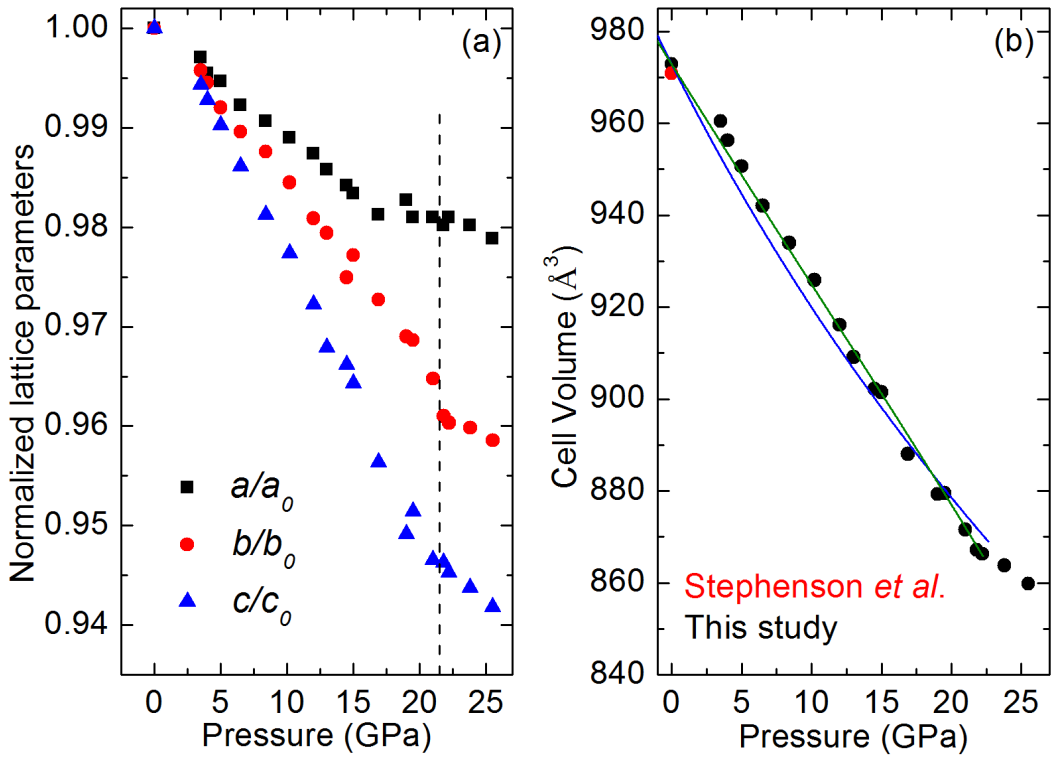

FIG. 4. (a) Pressure dependence of the normalized lattice parameters and (b) volume-pressure data for the L-Ta_2O_5. The solid green and blue lines are third- and second-order B-M equation of state unweighted fits respectively, of the HP phase experimental data.

Application of the F-f model to the data reveals that the pressure dependent stress, within the established errors, exhibits a linear response to applied strain (See Fig. 5(b)). There is no indication of a pressure or strain induced modification to the initial structure. The third-order B-M EOS yielded the statistically best representation of the data (See: Figure 5(a) and Table II). It is unusual that the first pressure derivative of the bulk modulus, K', has a value near zero; within the experimental error, the compressibility of Ta_2O_5 appears to be pressure invariant up to approximately 25 GPa.

The low value of K' as determined by both the unweighed and the weighed fits is relatively unusual, although low, or even negative,values of K' have been reported in the literature.[27,28] The complete elucidation of this aspect is beyond the scope of this paper as it may require singe crystal diffraction in order to accurately determine interatomic distances and also thermal expansion measurements. At the present level, we can speculate the following explanations: a) L-Ta_2O_5 crystal structure is characterized by extensive corner-sharings

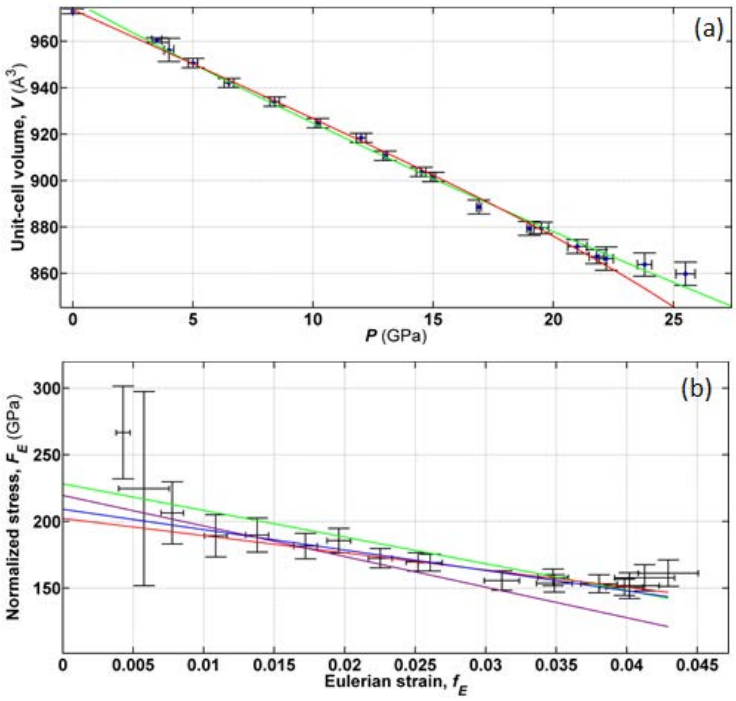

FIG. 5. (a) Third order Birch-Murnaghan EOS model weighted fit to Ta_2O_5 data. The red line represents a weighted fit and the green line is from an unweighted fit. b) First-order F-f EOS mode weighted fit to Ta_2O_5 data. The red line represents a weighted fit and the green line is from an unweighted fit. The violet line represents a weighted Vinet EOS fit and the blue line is from a third-order B-M EOS model fit to the data.

between TaO_x polyhedra with additional open space between the polyhedra. Consequently, the compressibility is mainly determined by the changes in Ta-O-Ta bond angles through rotation of multiple corner sharing polyhedra. This is in agrement with the experimentally observed higher compressibility of the c axis, see Figs. 1 and 4, the axis that is perpendicular to the O-Ta-O layers. Another way to describe the same scenario is the, almost negligible, repulsion between polyhedra as discussed in details in Ref..[22] b) Bragg peaks broadening, even during the initial step of compression, indicates that L-Ta_2O_5 exhibits a tendency for disorder even at low pressures. The proposed tendency for disorder is in agrement with the results of the Raman spectroscopy measurements by Li *et al.*[13] This is probably, due to pressure induced frustration and/or competition between different local orderings of the Ta sublattice, as XRD intensity is, almost entirely, dominated by Ta cations.

Now we turn our attention to the disagreement between the EOS reported in our study

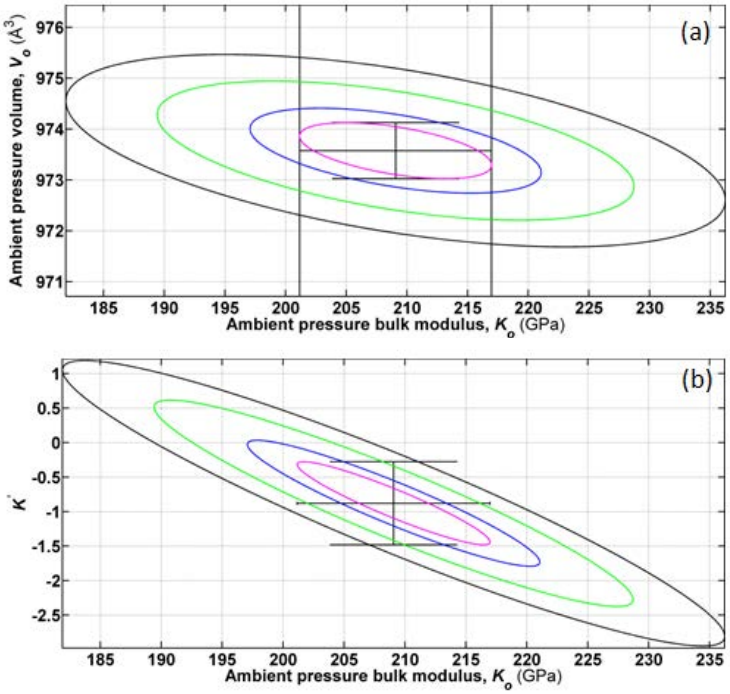

FIG. 6. Confidence ellipses from a third order Birch-Murnaghan EOS model weighted fit to Ta_2O_5 data. The magenta colored ellipse is 0.607-σ (50.3% confidence), blue is 1-σ (68.3% confidence), green is 2-σ (95.4% confidence), and the black ellipse is 3-σ (99.7% confidence).

TABLE II. Model EOS parameters derived from fits to our Ta_2O_5 data, unweighted and weighted according to experimental uncertainties. Note: *K"* (bracketed terms) is implied for 2nd and 3rd B-M and F(f) 1^{st} order results (See: O.L. Anderson, 1995 Oxford Univ. Press[26]).

Experimentally Weighted Fits											
B-M order	V_0(Å^3)	V_0 esd	K_0(GPa)	K_0 esd	K'	K' esd	K"	K" esd	χ^2_{red}	Max ΔP (GPa)	KS-test
2	982.11	1.97	142.49	3.92	4.00	0.00	[-0.03]	[0.00]	4.10	1.37	0.30
3	977.48	2.18	173.22	12.70	1.62	0.81	-0.05	[0.02]	[2.05]	1.40	0.21
4	972.91	1.40	247.70	19.36	-8.72	2.10	0.03	[0.07]	[1.29]	0.89	0.17
Vinet EOS	V_0	V_0 esd	K_0	K_0 esd	K'	K' esd	K"	K" esd	χ^2_{red}	Max ΔP	KS-test
	976.55 2.18	181.81	14.35	0.61	1.14	0.00	0.01	3.05	1.41	0.19	
F-f order	V_0	V_0 esd	K_0	K_0 esd	K'	K' esd	K"	K" esd	χ^2_{red}	Max ΔP	KS-test
1	972.87	0.97	179.56	9.51	1.73	0.80	[-0.04]	[0.02]	5.40	0.92	0.53

and the one reported by Li *et al.* . Although the authors in Ref.[13] state that they present a high pressure study of the low temperature orthorhombic Ta_2O_5 they adopt the T-Ta_2O_5 structure for indexing their XRD patterns and also the reported volumes and lattice parameters are in agrement with the one reported by Hummel *et al.*, see Table I. Given that the

authors used commercially available Ta_2O_5 powder, it is unlikely that the starting material is the T-Ta_2O_5 allotrope, normally synthesized under specific chemical and temperature conditions. As it can be clearly observed in Fig. 2(a), the calculated XRD patterns of L-Ta_2O_5 and T-Ta_2O_5 are hardy distinguishable based only on the positions and the relative intensities of the main Bragg peaks. This can be attributed to the common structural characteristics of these two allotropes,[10,12] see discussion in the introduction and Table I. However, a closer inspection of the lower intensity Bragg peaks, especially at low 2θ, can provide a way to distinguish between the XRD patterns of these structural modifications, see inset in Fig.2(a). Unfortunately, a refinement of the experimental patterns was not provided by the authors and moreover, the low angle part of the 2θ range ($<8^o$ in Ref. 1 and $< 6.4^o$ in Fig. 2(a)) is missing. Nevertheless, we believe that the measured XRD pattern by Li *et al.* can be rather indexed with the L-Ta_2O_5 structure. From the above discussion we can conclude that Li and coworkers made an unintentional error by indexing their experimental patterns with the T-Ta_2O_5 structure and thus, reporting an EOS that doesn't correspond to any crystal form of Ta_2O_5. Finally, it is plausible to assume that the higher critical pressure for amorphization in this study (26.5 GPa vs ∼21 GPa in Ref.[13]) can be attributed to the use of Neon in this study instead of the less hydrostatic above 10 GPa methanol-ethanol mixture used by Li *et al.*

IV. CONCLUSION

To summarize, the high-pressure structural behavior of Ta_2O_5 has been explored experimentally up to 28.3 GPa using synchrotron x-ray diffraction. We have shown that the ambient phase can be indexed with the "low-temperature" L-Ta_2O_5 structure. The L-Ta_2O_5 phase remains stable up to 25 GPa were a pressure induced amorphization takes place. The respective bulk moduli and corresponding pressure derivatives were derived from weighted and unweighted fits using selected (relatively optimal) EOS models. We have shown that Li and co-workers have unintentionally reported an erroneous high-pressure EOS for the low temperature phase of Ta_2O_5 based on the T-Ta_2O_5 phase.

ACKNOWLEDGMENTS

E. S. would like to thank K. Syassen for fruitful discussions and critical reading of the manuscript. This work was performed under the auspices of the U. S. Department of Energy by Lawrence Livermore National Security, LLC under Contract DE-AC52-07NA27344. We thank the Joint Munitions Program (JMP - TCG-III) for supporting this study and also the high explosives science campaign II research program at Lawrence Livermore National Laboratory. The Advanced Light Source is supported by the Director, Office of Science, Office of Basic Energy Sciences, of the U.S. Department of Energy under Contract No. DE-AC02-05CH11231.

REFERENCES

[1]M. H. Asghar, F. Placido, and S. Naseem, J. Phys. D: Appl. Phys. **40**, 2065 (2007).

[2]J. D. Prymak, in *Conference Record of 1998 IEEE Industry Applications Conference. Thirty-Third IAS Annual Meeting (Cat. No.98CH36242)*, Vol. 2 (1998) pp. 1129–1137 vol.2.

[3]E. L. Dreizin, Prog. Energy Combust. Sci. **35**, 141 (2009).

[4]C. W. Won, H. H. Nersisyan, H. I. Won, and J. H. Lee, Curr. Opin. Solid State Mater. Sci. **14**, 53 (2010).

[5]O. G. Cervantes, J. D. Kuntz, A. E. Gash, and Z. A. Munir, Combust. Flame **158**, 117 (2011).

[6]J. E. Miller, T. R. Boehly, D. A. Meyerhofer, and J. H. Eggert, in *Shock compression of condensed matter - 2007, pts 1 and 2*, AIP Conference Proceedings, Vol. 955, edited by M. Elert, M. Furnish, R. Chau, N. Holmes, and J. Nguyen (2007) pp. 71–74, Conference of the American-Physical-Society-Topical-Group on Shock Compression of Condensed Matter, Waikoloa, HI, JUN 24-29, 2007.

[7]G. Fenton, D. Grady, and T. Vogler, in *Shock compression of condensed matter - 2011, pts 1 and 2*, AIP Conference Proceedings, Vol. 1426, edited by M. Elert, W. Buttler, J. Borg, J. Jordan, and T. Vogler (2012) 7th Biennial Conference of the American-Physical-Society-Topical-Group on Shock Compression of Condensed Matter, Chicago, IL, JUN 26-JUL 01, 2011.

[8]J.-Y. Kim, B. Magyari-Koepe, K.-J. Lee, H.-S. Kim, S.-H. Lee, and Y. Nishi, Phys. Status Solidi Rapid Res. Lett **8**, 560 (2014).

[9]S. Perez-Walton, C. Valencia-Balvin, A. C. M. Padilha, G. M. Dalpian, and J. M. Osorio-Guillen, J. Phys.: Condens. Matter **28** (2016).

[10]N. Stephenson and R. Roth, Acta Crystallogr. Sect. B **B 27**, 1037 (1971).

[11]L. Aleshina and S. Loginova, Crystallogr. Rep. **47**, 415 (2002).

[12]H.-U. Hummel, R. Fackler, and P. Remmert, Chemische Berichte **125**, 551 (1992).

[13]Q. Li, H. Zhang, B. Cheng, R. Liu, B. Liu, J. Liu, Z. Chen, B. Zou, T. Cui, and B. Liu, J. Appl. Phys. **115**, 193512 (2014).

[14]M. Matsui, International Conference On High Pressure Science and Technology, Joint AIRAPT-22 and HPCJ-50 **215**, 012197 (2010).

[15]K. Syassen, High Pres. Res. **28**, 75 (2008).

[16]M. Kunz, A. MacDowell, W. Caldwell, D. Cambie, R. Celestre, E. Domning, R. Duarte, A. Gleason, J. Glossinger, N. Kelez, D. Plate, T. Yu, J. Zaug, H. Padmore, R. Jeanloz, A. Alivisatos, and S. Clark, J. Synchrotron Radiat. **12**, 650 (2005).

[17]C. Prescher and V. B. Prakapenka, High Pres. Res. **35**, 223 (2015).

[18]W. Kraus and G. Nolze, J. Appl. Crystallogr. **29**, 301 (1996).

[19]A. C. Larson and R. B. V. Dreele, "GSAS: General structure analysis system report LAUR 86-748," Tech. Rep. (Los Alamos National Laboratory, 2000).

[20]A. Boultif and D. Louër, J. Appl. Crystallogr. **37**, 724 (2004).

[21]F. Birch, J. Geophys. Res. **83**, 1257 (1978).

[22]E. Stavrou, M. R. Manaa, J. M. Zaug, I.-F. W. Kuo, P. F. Pagoria, B. Kalkan, J. C. Crowhurst, and M. R. Armstrong, The Journal of Chemical Physics **143**, 144506 (2015).

[23]P. Vinet, J. Ferrante, J. R. Smith, and J. H. Rose, J. Phys. C **19**, L467 (1986).

[24]F. Birch, Phys. Rev. **71**, 809 (1947).

[25]R. J. Angel, Rev. Mineral Geochem. **41**, 35 (2000).

[26]O. Anderson, *Equations of State of Solids in Geophysics and Ceramic Science* (Oxford University Press Inc, 1995).

[27]I. Efthimiopoulos, T. Lochbiler, V. Tsurkan, A. Loidl, V. Felea, and Y. Wang, J. Phys. Chem. C **0**, null (2017).

[28]H. Fang and M. T. Dove, Phys. Rev. B **87**, 214109 (2013).